基于相变材料的非易失光子多值器件研究

宋兵,王金融,张亨宇,孙振源,李清江

（国防科技大学 电子科学学院,长沙 410073）

摘　要：结合相变材料与马赫-曾德尔干涉仪调制器结构,设计了一种包含 ITO 微加热器的非易失性光子多值器件,通过对相变材料的结构参数进行仿真,优化了器件的调制窗口。同时对 ITO 微加热器的结构进行仿真设计,使微加热器的效率更高,更容易实现器件的多值调制。测试表明,该器件在施加电脉冲的过程中实现了超过 32 个状态（5 bit）的多值调制。这种电调制的非易失性光子多值器件为大规模的非易失性可配置光子硬件神经网络提供了基础的单元。

关键词：非易失性；光子器件；马赫-曾德尔干涉仪；相变材料；硒化锑；氧化铟锡；多值

中图分类号：TN256　　　　**文献标识码**：A　　　　　　**doi**：10.3788/gzxb20245301.0123001

0　引言

　　人工智能[1-2]的蓬勃发展对计算系统提出了更高的要求,急需发展新的高速度高能效计算硬件。近年来,以 Chat GPT 为代表的人工智能大模型对算力的需求每 3～4 个月翻一番[3],当前的人工智能处理硬件主要采用图形处理器（Graphics Processing Unit, GPU）,英伟达最先进的图形处理器算力能够达到 80 tera FLOPS[4]。以图形处理器为代表的电子计算系统采用冯诺依曼架构,其处理器与存储器分置导致运算过程中频繁搬移数据产生大量的能量消耗,上述所说的图形处理器功耗超过 400 W,且电子计算系统中的寄生电容影响了计算速度的进一步提高,无法满足人工智能进一步发展对高速度高能效的计算硬件需求[5-6]。

　　基于集成光子器件的光子智能加速器快速发展[7-8],为实现高速度高能效的计算硬件提出了一种可行的解决方案。基于马赫-曾德尔干涉仪（Mach-Zehnder Interferometer, MZI）[9-13]的可调多值器件是当前构成光子智能加速器的一种主要技术途径,该类器件具备宽带宽和温度不敏感的优势,使其成为光子硬件加速器的优越选择。但是,该类器件的多值特性是通过热光效应[14-15]和载流子迁移[16-17]来实现调制的,其产生的相移通常都比较小,导致器件的尺寸较大,不利于大规模的集成,同时器件具有易失性,无法长时间保持多值,增加了调制的能量需求。利用相变材料（Phase Change Material, PCM）[18-25]的折射率连续可调且非易失保持的特性,将相变材料与上述器件结合能够实现非易失保持的多值特性,为构建光子智能加速器提供一种新的器件基础。

　　本文实现了一种基于 SbSe 相变材料的非易失性多值器件,首先通过 Lumerical 仿真优化了相变材料长度和厚度等结构参数,在此基础上制备了器件,测试过程中通过对微加热器施加电脉冲对相变材料进行调制,实现了器件的多值特性。

1　器件设计

1.1　结构设计

　　本文设计的多值器件结构如图 1(a)所示,主要由马赫-曾德尔干涉仪、相变材料、微加热器和调制电极构成。其中,马赫-曾德尔干涉仪设计成单输入单输出结构,脊波导的脊高 120 nm,宽 500 nm,底厚 100 nm,

http://www.photon.ac.cn

(a) Device structure diagram

(b) Electric field distribution in ridge waveguide

(c) Heat distribution on top of block microheater
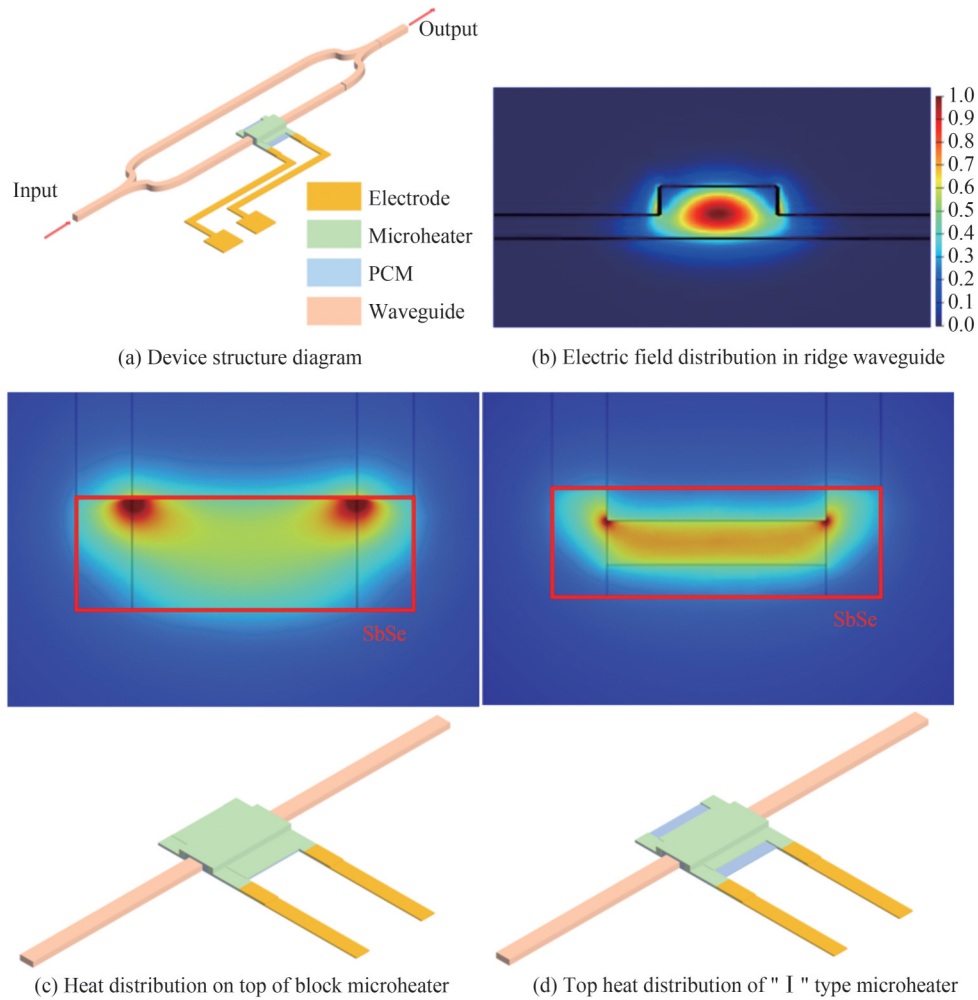
(d) Top heat distribution of "Ⅰ" type microheater

图 1 器件结构与仿真

Fig. 1 Device structure and simulation

用于 1 550 nm 波长的光单模传输,并且传输模式能够很好的限制在波导的内部,如图 1(b)。在马赫-曾德尔干涉仪器件的一条臂上覆盖 SbSe 相变材料,SbSe 相变材料在 1 550 nm 波段附近的消光系数接近 0,晶态和非晶态的折射率分别为 4.05 和 3.285,折射率差异超过 0.7[26],可用于实现多值相位调制。然后在相变材料上覆盖一层 120 nm 厚的氧化铟锡(Indium Tin Oxides,ITO)作为微加热器,其具有导电性好和 1 550 nm 光吸收弱的特点,在工作过程中通过 ITO 的电脉冲产生焦耳热,从而改变相变材料的温度诱导其发生相变。采用 ITO 作为微加热器的方案相比热退火的方案具有调制速度更快、调制精细度更高的优势,能够在毫秒级的时间内实现器件的状态转换。电极是在 ITO 两端的边缘上覆盖 10 nm/120 nm 厚的 Cr/Au 形成。

在设计过程中,微加热器的热分布对相变材料相变具有重要影响,本文设计了两种不同的微加热器结构并通过 COMSOL 进行电流和固体传热仿真,验证热量的分布情况。首先,微加热器设计成方块型,如图 1(c),仿真显示这种微加热器结构在施加电脉冲时产生的热量分布比较分散,无法将热量集中到相变材料上。为了使产生的热量更加集中,微加热器的形状被设计成了两边宽中间窄的"工"字型,这样的结构可以使得电流产生的焦耳热集中到微加热器的中间部分,如图 1(d),仿真显示了在施加电压脉冲时微加热器顶部的热量分布,可见热量集中在相变材料部分,并且向其余部分逸散的较少,有利于引导相变材料产生相变。

1.2 结构参数优化

采用 Lumerical 软件中的 2.5D 有限元分析(varFDTD)对器件的传输进行了模拟仿真,研究了器件不同参数下的光传输性能。首先,在软件中设置了上述器件结构,从其输入端输入波长 1 500 nm～1 600 nm 的连续光,在输出端检测光通过率。其次,为了观察相变材料相变过程中器件输出的变化,在仿真中固定相变材料的长度,其在长度方向包含晶化和非晶化两种状态的相变材料,连续改变两者的占比,使其从完全晶化逐渐转变

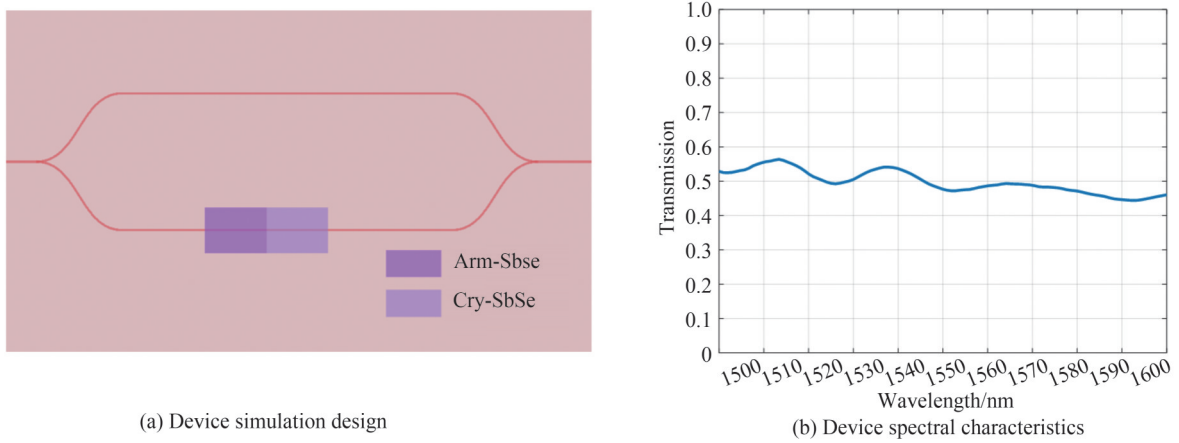为完全非晶化,观察器件光通过率的变化规律,仿真设置如图2(a)所示。MZI器件具有宽带性的特点[27],图2(b)展示了器件在晶化占比50％时的光谱特性仿真结果,可见器件确实在不同波长的输出变化不大。

(a) Device simulation design

(b) Device spectral characteristics

图2　器件仿真设计与光谱特性

Fig. 2　Device simulation design and spectral characteristics

分析相变材料长度对器件的影响时,固定相变材料的厚度为30 nm,仿真得到其20 μm～50 μm四个长度器件的通过率变化,1 550 nm波段时结果如图3所示,其中横轴代表的是相变材料的非晶化程度,纵轴代表器件的通过率。图3(a)中相变材料长度为20 μm时,相变材料非晶化过程中,器件的通过率从0.2先降低到0左右,再增加到0.65,此时器件的窗口明显增大。图3(b)中相变材料长度为30 μm时,相变材料非晶化

(a) 30 nm thickness, 10 μm length

(b) 30 nm thickness, 20 μm length

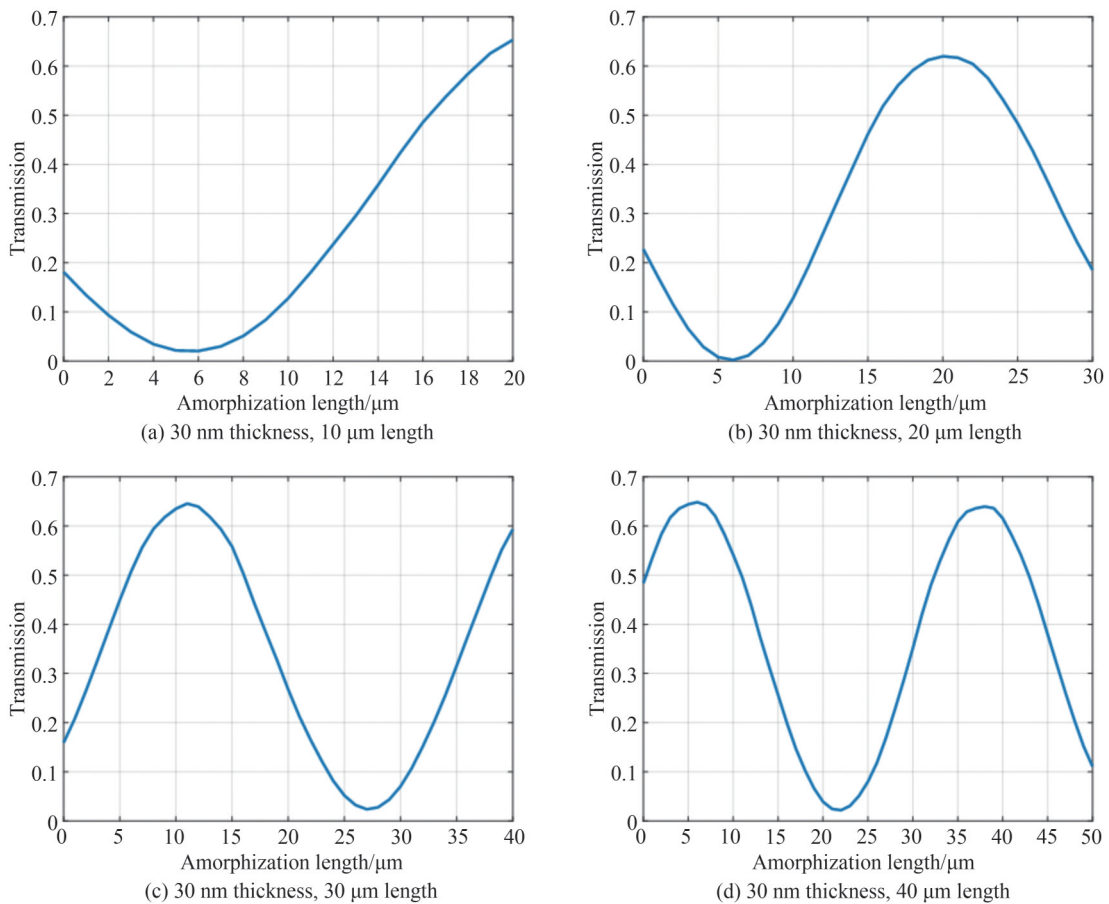(c) 30 nm thickness, 30 μm length

(d) 30 nm thickness, 40 μm length

图3　相变材料长度仿真

Fig. 3　Length simulation of phase change materials

过程中,器件的通过率从0.2降低到0,再增加到0.6,最后降低到0.2,经历了一个周期性变化,说明器件的窗口达到了2Π。图3(c)中相变材料长度为40 μm时,器件的通过率变化超过了一个周期,超过2Π的部分并不会使器件的性能进一步提高,并且过长的相变材料导致调制难度增大和器件尺寸增大。图3(d)中可见,当器件窗口超过2Π时存在的两个极大值大小几乎相同,进一步证明过长的相变材料不会使器件的性能提高。

分析相变材料厚度对器件的影响时,固定相变材料的长度为30 μm,仿真得到10 nm～40 nm四个厚度器件的通过率变化。图4(a)～(d)分别展示了相变材料厚度从10 nm到40 nm的仿真结果。与研究相变材料长度时的结果相似,当厚度逐渐增加时,器件通过率变化的窗口逐渐增大。因此综合分析,选取长度30 μm和厚度30 nm作为相变材料的参数进行器件制备,此参数下器件窗口刚好超过2Π。

(a) 30 μm Length, 10 nm thickness

(b) 30 μm Length, 20 nm thickness
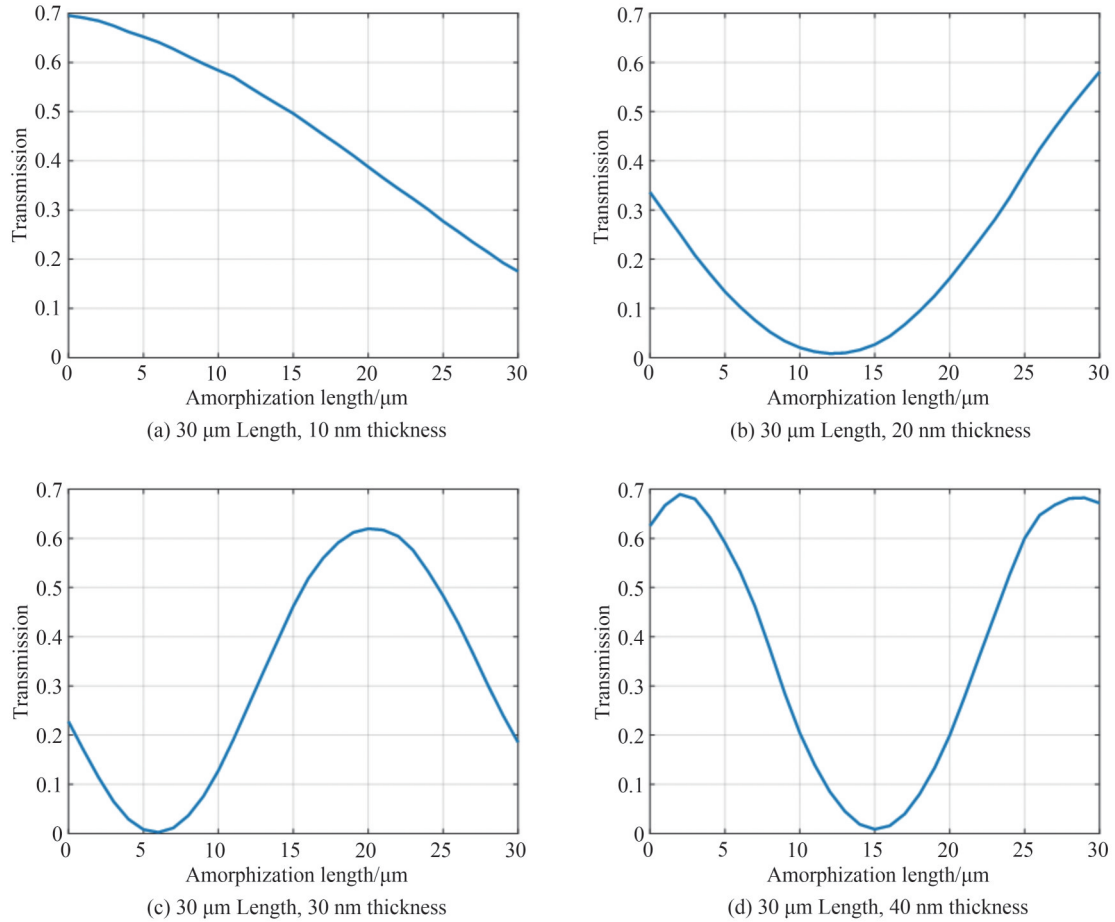
(c) 30 μm Length, 30 nm thickness

(d) 30 μm Length, 40 nm thickness

图4 相变材料厚度仿真
Fig. 4 Thickness simulation of phase change materials

2 器件制备与测试

2.1 器件制备

第一步准备清洗干净的SOI(顶层硅-氧化层-基底厚度为220 nm-2 μm-675 μm),第二步使用电子束光刻的正胶工艺将波导图形转移到SOI上,用电感耦合等离子体刻蚀(Inductive Coupled Plasma Emission Spectrometer,ICP)的方法形成脊波导,第三步使用紫外光刻负胶工艺将相变材料的图形转移到脊波导上方,用磁控溅射方法在脊波导上沉积SbSe,厚度为30 nm,刚生长制备的SbSe的初始状态为非晶态。然后重复使用紫外光刻和磁控溅射在SbSe上方沉积120 nm厚的ITO,以及在ITO两端形成电极,电极使用10 nm的Cr和120 nm的Au。图5(a)为器件制备流程图。使用金相显微镜对制备完成的器件进行表征,如图5(b),器件结构符合设计预期。

(a) Device preparation process

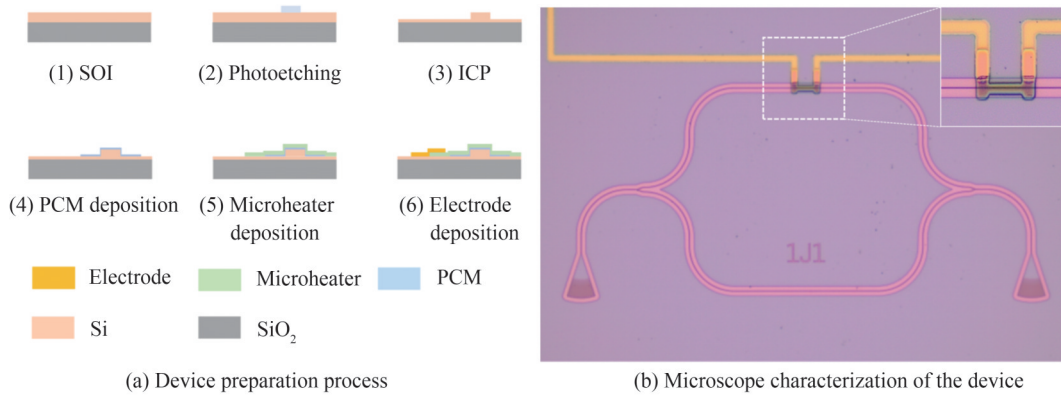(b) Microscope characterization of the device

图5 器件制备流程及显微镜表征

Fig. 5 Device preparation process and microscope characterization diagram

2.2 多值测试

本实验采用的测试系统分为测试光路与调制电路两部分，如图6(a)所示，其中可调谐激光器用于施加测试光，半导体参数分析仪用于施加电脉冲。测试光路由激光器、偏振控制器、光纤阵列、光电探测器、数据采集卡组成，激光器输出的测试光先经过偏振控制器，再通过光纤阵列进入器件的输入端，再从输出端进入到光纤阵列中，连接到探测器，将光信号转变为电信号，最后在数据采集卡中采集下来。调制电路由半导体分析仪和电探针组成，在半导体分析仪中设置电脉冲参数，将电探针与调制电极接触，电脉冲通过电探针与调制电极，实现器件调制。为了诱导相变材料相变，施加电脉冲后微加热器产生的热量必须满足相变材料达到其相变温度。

(a) Device test system

(b) Device test result

(c) Device retention characteristic
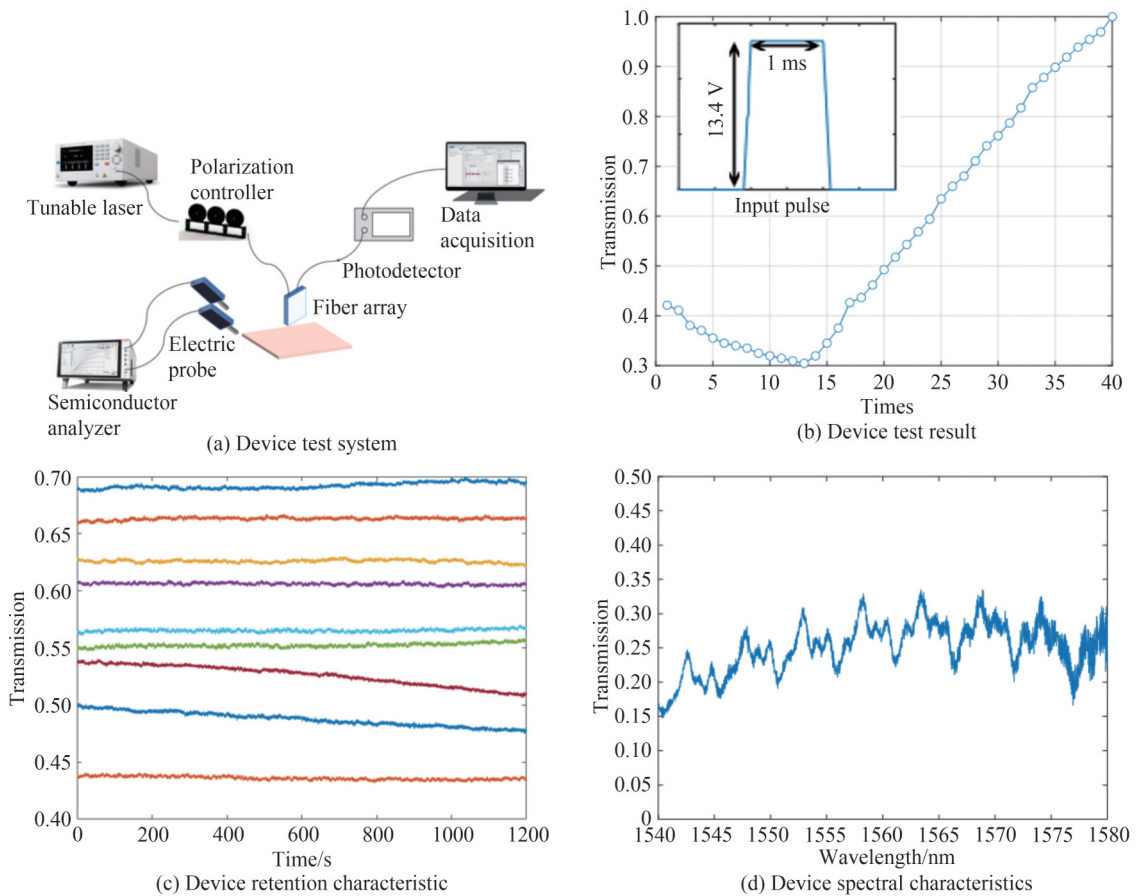
(d) Device spectral characteristics

图6 器件测试系统与测试结果

Fig.6 Device test system and test results

在测试过程中,相变材料的初始状态为非晶态,为了使相变材料实现晶化,需要施加一个低电压的宽脉冲,使相变材料达到晶化温度并保持一段时间使晶格有序化。对于该器件,施加一个宽度为 1 ms,幅度为 13.4 V 的方形脉冲可以实现晶化。图 6(b)为器件输出功率与调制次数之间的关系。在施加电压的过程中,器件的通过率从 0.4 先减小至 0.3,然后逐渐增大到 1,变化规律符合马赫-曾德尔干涉仪器件由于两臂相位差连续变化导致输出连续正弦变化的特性,可以得出器件在调制过程中由于微加热器的电热效应使相变材料晶化,实现了器件的多值特性,状态数超过 32 个。

然而,继续提高电脉冲的能量,由于 ITO 表面温度与底部温度分布不均匀,导致顶层 ITO 温度过高致使熔断,无法进一步实现器件的完全晶化,没有达到器件仿真中预期的 2Π 窗口。并且为了实现器件的非晶化,需要施加高电压的窄脉冲,使相变材料达到融化温度并迅速冷却,这个过程中 ITO 微加热器同样会熔断,导致器件无法实现非晶化。如果要进一步实现器件的非晶化,需要改变微加热器的材料选型以及结构,比较有希望的是采用 PIN 微加热器的方案,由于其结构是直接形成于 SOI 内部的,耐用性和热稳定性更好,对于实现相变材料的非晶化问题具有很大的潜力。

图 6(c)为器件的保持特性测试,从器件多值特性测试中选取了若干个值进行测试,每间隔 0.1 s 进行一次数据采集,每个状态测试了 20 min,测试表明器件输出能够长时间保持稳定,即具有非易失性。

使用激光器在 1 540 nm~1 580 nm 波长范围对光子多值器件以及直波导进行扫描,直波导所获得的光谱为光栅耦合器的光谱。因此将多值器件的光谱与光栅耦合器的光谱进行数据处理,去除光栅耦合器的影响得到器件本身的光谱特性如图 6(d)。器件在这个波长范围内的输出比较稳定,具有一定的宽带特性,为实现并行计算提供了基础。上述多值器件能够作为光子计算单元进行精确的权值表示,适用于大规模的非易失性可重构光子计算网络,不需要频繁的配置。

3 结论

本文提出了一种基于 SbSe 的非易失性光子多值器件,通过有限元分析优化了器件的结构参数,使其完全相变时能够使窗口达到最大。通过在微加热器的两侧施加电脉冲来诱导晶化过程,该器件实现了超过 32 个态的多值调制,对非易失性光子加速器的发展具有重要意义,为构建光子智能加速器提供了一种新的解决方案。在未来通过寻找新的微加热器有望使该器件的性能进一步提高,实现功耗更低、可调状态数更多的光子多值器件。

参考文献

[1] SHASTRI B J, TAIT A N, FERREIRA DE LIMA T, et al. Photonics for artificial intelligence and neuromorphic computing[J]. Nature Photonics, 2021, 15(2): 102-114.

[2] GOI E, ZHANG Q, CHEN X, et al. Perspective on photonic memristive neuromorphic computing[J]. PhotoniX, 2020, 1: 1-26.

[3] AMODEI D, HERNANDEZ D D. AI and compute[OL]. https://blog.openai.com/ai-and-compute/.

[4] NVIDA. NVIDIA A100 tensor core GPU[OL]. https://images.nvidia.cn/aem-dam/en-zz/Solutions/data-center/a100/nvidia-a100-datasheet-nvidia-a4-2188504-r5-zhCN.pdf.

[5] FELDMANN J, YOUNGBLOOD N, KARPOV M, et al. Parallel convolutional processing using an integrated photonic tensor core[J]. Nature, 2021, 589(7840): 52-58.

[6] ASHTIANI F, GEERS A J, AFLATOUNI F. An on-chip photonic deep neural network for image classification[J]. Nature, 2022, 606(7914): 501-506.

[7] TAN J Y S, CHENG Z, FELDMANN J, et al. Monadic Pavlovian associative learning in a backpropagation-free photonic network[J]. Optica, 2022, 9(7): 792-802.

[8] ZHANG W, HUANG C, PENG H T, et al. Silicon microring synapses enable photonic deep learning beyond 9-bit precision[J]. Optica, 2022, 9(5): 579-584.

[9] PÉREZ D, GASULLA I, CRUDGINGTON L, et al. Multipurpose silicon photonics signal processor core[J]. Nature Communications, 2017, 8(1): 636.

[10] MARPAUNG D, YAO J, CAPMANY J. Integrated microwave photonics[J]. Nature Photonics, 2019, 13(2): 80-90.

[11] ZHU C, LU L, SHAN W, et al. Silicon integrated microwave photonic beamformer[J]. Optica, 2020, 7(9): 1162-1170.

[12] ZHOU H, ZHAO Y, WANG X, et al. Self-configuring and reconfigurable silicon photonic signal processor[J]. Acs Photonics, 2020, 7(3): 792-799.

［13］ ZHENG S, LONG Y, GAO D, et al. Chip-scale reconfigurable optical full-field manipulation：enabling a compact grooming photonic signal processor[J]. ACS Photonics, 2020, 7(5)：1235-1245.

［14］ XIAO X, PROIETTI R, LIU G, et al. Silicon photonic Flex-LIONS for bandwidth-reconfigurable optical interconnects[J]. IEEE Journal of Selected Topics in Quantum Electronics, 2019, 26(2)：1-10.

［15］ XIE Y, SHI Y, LIU L, et al. Thermally-reconfigurable silicon photonic devices and circuits[J]. IEEE Journal of Selected Topics in Quantum Electronics, 2020, 26(5)：1-20.

［16］ QIAO L, TANG W, CHU T. 32×32 silicon electro-optic switch with built-in monitors and balanced-status units[J]. Scientific Reports, 2017, 7(1)：42306.

［17］ DUPUIS N, DOANY F, BUDD R A, et al. A 4×4 electrooptic silicon photonic switch fabric with net neutral insertion loss[J]. Journal of Lightwave Technology, 2019, 38(2)：178-184.

［18］ WUTTIG M, BHASKARAN H, TAUBNER T. Phase-change materials for non-volatile photonic applications[J]. Nature Photonics, 2017, 11(8)：465-476.

［19］ FANG Z, CHEN R, ZHENG J, et al. Non-volatile reconfigurable silicon photonics based on phase-change materials[J]. IEEE Journal of Selected Topics in Quantum Electronics, 2021, 28(3)：1-17.

［20］ PARRA J, OLIVARES I, BRIMONT A, et al. Toward nonvolatile switching in silicon photonic devices[J]. Laser & Photonics Reviews, 2021, 15(6)：2000501.

［21］ ZHANG Y, FOWLER C, LIANG J, et al. Electrically reconfigurable non-volatile metasurface using low-loss optical phase-change material[J]. Nature Nanotechnology, 2021, 16(6)：661-666.

［22］ AGGARWAL S, MILNE T, FARMAKIDIS N, et al. Antimony as a programmable element in integrated nanophotonics[J]. Nano Letters, 2022, 22(9)：3532-3538.

［23］ ZHANG H, WANG X, ZHANG W. First-principles investigation of amorphous Ge-Sb-Se-Te optical phase-change materials[J]. Optical Materials Express, 2022, 12(7)：2497-2506.

［24］ CHENG Z, RÍOS C, PERNICE W H, et al. On-chip photonic synapse [J]. Advanced Science, 2017, 3：e1700160.

［25］ CHENG Z, RÍOS C, YOUNGBLOOD N, et al. Device-level photonic memories and logic applications using phase-change materials[J]. Advanced Materials, 2018, 30(32)：1802435.

［26］ DELANEY M, ZEIMPEKIS I, LAWSON D, et al. A new family of ultralow loss reversible phase-change materials for photonic integrated circuits：Sb2S3 and Sb2Se3[J]. Advanced Functional Materials, 2020, 30(36)：2002447.

［27］ AMIN R, MAITI R, GUI Y, et al. Heterogeneously integrated ITO plasmonic Mach-Zehnder interferometric modulator on SOI[J]. Scientific Reports, 2021, 11(1)：1287.

Non-volatile Photonic Multilevel Devices Based on Phase Change Materials

SONG Bing, WANG Jinrong, ZHANG Hengyu, SUN Zhenyuan, LI Qingjiang

(*College of Electronic Science and Engineering*, *National University of Defense Technology*, *Changsha* 410073, *China*)

Abstract：The rapid development of artificial intelligence has posed new and higher demands on computing systems. Electronic computing systems, represented by Graphics Processors Unit(GPU), adopt the von Neumann architecture, which results in frequent data migration and high energy consumption due to the separation of processors and memory. The parasitic capacitance in electronic computing systems also hinders further improvement in computing speed, making it unable to meet the needs of further development of artificial intelligence for high-speed and high-efficiency computing hardware. The rapid development of integrated photonic devices has provided a feasible solution for achieving high-speed and high-efficiency computing hardware. The tunable multivalued devices based on Mach-Zehnder interferometers are a major technological approach in constructing photonic intelligent accelerators. These devices have the advantages of wide bandwidth and temperature insensitivity, making them an excellent choice for photonic hardware accelerators. Phase-change materials have the characteristics of continuously adjustable refractive index and non-volatile retention. Combining phase-change materials with Mach-Zehnder interferometers can achieve non-volatile multivalued properties, providing a new device foundation for constructing photonic intelligent accelerators. In this paper, a non-volatile photonic multivalued device with an Indium Tin Oxides (ITO) microheater is designed based on the combination of

phase-change materials and Mach-Zehnder interferometer modulators. First, the structure of the photonic multivalued device is designed. Sb_2Se_3 is chosen as the phase-change material, and ITO is selected as the microheater material. The Sb_2Se_3 is deposited on one arm of the Mach-Zehnder interferometers waveguide, and ITO is deposited on top of the Sb_2Se_3. Cr/Au is deposited at the edge of the ITO to form electrodes. When the state of Sb_2Se_3 changes, it affects the phase of the transmitted light on the Mach-Zehnder interferometers waveguide, thereby changing the output of the Mach-Zehnder interferometers. This scheme has the advantages of faster modulation speed and higher modulation precision, enabling state transitions of the device to be achieved in milliseconds. The thermal distribution of the microheater has an important influence on the phase transition of the phase-change material. Two different microheater structures are designed and simulated using COMSOL software, including a square-shaped ITO and a structure with wider edges and a narrower middle. Through electrical-thermal simulations, it is found that the second structure can concentrate the generated heat more effectively and improve the efficiency of the microheater. Furthermore, the length and thickness parameters of Sb_2Se_3 are optimized through simulations in Lumerical software. Lengths ranging from 20 μm to 50 μm and thicknesses ranging from 10 nm to 40 nm are chosen. Finally, a length of 30 μm and a thickness of 30nm are determined as the optimal parameters for Sb_2Se_3, which maximize the modulation window of the device. The device is fabricated using processes such as photolithography, magnetron sputtering, and inductively coupled plasma etching. During the testing process, electrical pulses are applied to the microheater, with a pulse width of 1ms and an amplitude of 13.4 V. The tests demonstrate that the device achieves multivalued modulation with over 32 states (5 bits) during the application of electrical pulses. Several states are also selected for the retention characteristic tests, which show that the device can maintain stable states for up to 20 minutes, indicating good non-volatility. Finally, the spectral characteristics of the photonic multivalued device are tested to determine its bandwidth. The tests show that the output of the device remains stable between 1 540 nm and 1 580 nm, indicating certain broadband characteristics and providing a foundation for parallel computing. This electrically modulated non-volatile photonic multivalued device serves as a fundamental unit for large-scale non-volatile reconfigurable photonic hardware neural networks. In the future, the performance of this device can be further improved by exploring new microheater designs, aiming for lower power consumption and more adjustable states in photonic multivalued devices.

Key words：Nonvolatile；Photonic devices；Mach-Zehnder interferometer；Phase change material；SbSe；ITO；Multi-level

OCIS Codes：130.1750；130. 3130；130.0250